HiLL PUBLISHING

OAJRC Material Science, 2024, 6(1), 12-18
http://www.hillpublisher.com/journals/oajrcms/
ISSN Online: 2632-2072

Microstructure and Mechanical Properties of Multi-interface Tungsten Fibre/Aluminium Alloy Composites Prepared by Spark Plasma Sintering

Linhui Zhang[1,2,*], Yonghong Xu[1,2], Binnian Zhong[1,2]

[1]Qinghai Provincial Key Laboratory of New Light Alloys, Xining, Qinghai, China.
[2]Engineering Research Center of High Performance Light Metal Alloys and Forming, Qinghai University, Xining, Qinghai, China.

How to cite this paper: Linhui Zhang, Yonghong Xu, Binnian Zhong. (2024) Microstructure and Mechanical Properties of Multi-interface Tungsten Fibre/Aluminium Alloy Composites Prepared by Spark Plasma Sintering. *OAJRC Material Science*, 6(1), 12-18.
DOI: 10.26855/oajrcms.2024.06.002

Received: May 22, 2024
Accepted: June 19, 2024
Published: July 16, 2024

***Corresponding author:** Linhui Zhang, Qinghai Provincial Key Laboratory of New Light Alloys, Xining, Qinghai, China; Engineering Research Center of High Performance Light Metal Alloys and Forming, Qinghai University, Xining, Qinghai, China.

Abstract

There are hidden dangers in the use of stainless steel and fiber cement-based composite materials as the materials of disposal tanks, because of the accident of several nuclear leakage events in the world. The titanium alloy, nickel alloy and copper alloy also cannot guarantee the safety of nuclear waste due to the electrochemical corrosion at the weld, acid corrosion and chloride ion corrosion. Aluminum alloy was identified as a candidate material in the nuclear safety field by researchers as early as the 1980s due to its small specific absorption section, corrosion resistance and low price. However, the strength and density of Al alloy need to be improved for the materials used in disposal tanks. To enhance the strength and density of Aluminum alloy, tungsten fibre reinforced 7075 Al alloy composites with different content of tungsten fibre were produced by spark plasma sintering method. The mass percent of tungsten fibre in the composites are 5%, 10%, 15%, and 20%, respectively. Accordingly, the volume ratios of tungsten fibre are 0%, 5.11%, 10.19%, 15.27%, and 20.33%. The results show that all the composites have ideal interfacial bonding. The relative density of 5% tungsten fibre/7075 Aluminum alloy composite is as high as 98.83%. The distribution of tungsten fibre is reasonably more uniform with the increase in tungsten fibre content. Tensile tests indicate that the 10% tungsten fibre/7075 Aluminum alloy composite exhibits the largest strength, about 250 MPa. It is 72.4% higher than that of pure 7075 Al, which can be ascribed to the enhanced behavior of tungsten fibre. The hardness of the matrix was only between 50 and 60 HV, even smaller than that of fibre (about 1100 HV) and interface (1400 HV).

Keywords

Tungsten Fibre Reinforced, Metallic Composites, Spark Plasma Sintering, Interfaces

1. Introduction

Nuclear industry is growing at a very rapid rate and proper disposal of high-level radioactive waste is of great significance for ensuring nuclear power safety and social stability [1]. Candidate materials for high-level radioactive waste disposal tanks mainly considered include stainless steel, titanium alloy, nickel alloy, copper alloy, and fiber cement-based composite materials [2]. However, there are hidden dangers in the use of stainless steel [3] and fiber cement-based composite materials [4] as the materials of disposal tanks, because of the accident of several nuclear leakage events in the world. The titanium alloy, nickel alloy, and copper alloy also cannot guarantee the safety of nuclear waste due to the electrochemical corrosion at the weld [4], acid corrosion [5], and chloride ion corrosion [6]. There is an increasing demand for high-level radioactive waste disposal tank materials.

Aluminum (Al) alloy was identified as a candidate material in the nuclear safety field by researchers as early as the 1980s due

to its small specific absorption section, corrosion resistance, and low price [7]. However, the strength and density of Al alloy need to be improved for the materials used in disposal tanks. 7075 Al alloy possesses perfect corrosion resistance, good toughness, and higher strength than other Al alloy [8]. If improved the strength of 7075 Al alloy, maybe it will become the candidate material for high-level radioactive waste disposal tanks. Tungsten fibre (Wf) is an ideal fiber-reinforced material with high density, high strength, superior toughness, radiation resistance and corrosion resistance [9]. Wf/7075Al composites with the Wfs as reinforcement and the 7075 Al alloy as matrix could have advantages of both materials, such as high strength, ductility, toughness, and excellent corrosion resistance properties.

The spark plasma sintering (SPS) method is of great contribution to the powder metallurgy industry. SPS is a processing method at lower temperatures (compared with other powder metallurgy methods), low voltage, and in short periods (2 ~ 10 min) possible by discharging between the power particles surface and/or secondary, and it effectively performs a high-temperature spark plasma generated at an initial stage, which provides fast heating rate [14]. Owing to SPS, the degree of inter-diffusion between 7075 Al power particles and Wfs would increase. The Wf/7075Al composite has high strength due to its high density and fine grains by SPS. In this study, the short Wfs reinforced 7075 Al (Wf/7075Al) composites were fabricated by SPS technique. The effects of the short Wfs on the microstructure, tensile properties, and Vickers hardness of the Wf/7075Al composites were investigated in comparison with the pure 7075 Al sample.

2. Experimental section

The powder of 7075 Al (10 ~ 20 μm, purity > 99.9%) used in this test was purchased from Shanghai Chaowei Nanotechnology Co., Ltd. The chemical content of the powder was listed in Tab. 1, and the content was in compliance with the usage regulations (China GB/T3190-2008). The Wfs with a diameter of 75 μm were used as reinforcement and were obtained from Honglu Molybdenum Company, the chemical composition and mechanical properties were given in our previous work [15]. The short Wfs with length of 2-6 mm were cut by hydraulic shear, then chemically cleaned and stoved for 60 min at low temperature.

The short Wfs were buried into 7075 Al powders, and the test-selected mass ratio calculation method was used to calculate the mass of Wfs. The mass ratios of Wfs in Wf/7075Al composites were set to 0%, 5%, 10%, 15%, and 20%, and the volume ratios of

Wfs were 0%, 5.11%, 10.19%, 15.27%, and 20.33%. The physically mixed samples in graphite die were sintered by SPS (FCT Group, SE-607, Germany). It took 6 min to raise the temperature from room to 200 ℃, meanwhile, it improved pressure to 50 MPa. In the next 5 min, it was raised the temperature to 450 ℃ that hold for 10 min. Finally, it was cooled down to room temperature at the rate of 100 ℃/min. The sintered composite samples are 20 mm in diameter and about 2 mm in thickness containing the mass fractions 0%, 5%, 10%, 15%, and 20%Wfs, which are designated as 7075 Al, 5%Wf/7075Al, 10%Wf/7075Al, 15%Wf/7075Al and 20%Wf/7075Al, respectively.

Table 1. Chemical composition of 7075 Al alloy (% by mass)

Powder	Fe	Si	Cu	Mg	Mn	Zn	Al	other
7075 Al alloy %	0.153	0.280	1.533	2.324	0.130	5.720	89.81	<0.05

The density of Wf/7075Al composite was determined by Archimedes principle and the relative density was calculated by taking the theoretical density of Wfs and 7075 Al as 19.3 g/cm3 and 2.8 g/cm3. The sintered samples were polished and chemically etched by Keller reagent. The etched sections were examined using X-ray diffraction (XRD), optical microscopy (OM, ZEISS - AX10), and energy dispersive spectrometer (EDS) to investigate the phases, the distribution of the Wf, and the interface in the composites. The dog-bone-shaped tensile samples were cut, there was a working length of 5 mm and a cross-section of 1.5 × 1.5 mm2. Tensile experiments were carried out at room temperature using an Instron - 5967 machine with a constant displacement rate of 0.1 mm/min. The Wfs and 7075 Al matrix of samples were subjected to Vickers micro-hardness testing at room temperature with a load of 200 g on the matrix and 500g on the Wf and interface. There was a dwell time of 10 seconds by a Vickers Indenter.

3. Results and discussion

3.1 Phase analysis

The phase compositions of the composites with different Wfs mass fractions are shown in Fig. 1. All diffraction peaks correspond to the W or Al phase. The diffraction peak of the composites is consistent with that of a PDF standard card. In particular, the diffraction peaks of Al with a diffraction angle of 38.610°, 44.833°, 65.186°, 78.306°, 82.352° were obtained, and the indices of

lattice plane (111), (200), (220), (311) and (222) were obtained, respectively. Meanwhile, the diffraction peaks of W in the composites with a diffraction angle of 40.416°, 58.357°, 73.330°, 86.907°, indices of lattice plane (110), (200), (211), and (220), were obtained. But with the increase of Wfs content, the diffraction peaks of Al in the composites all shifted to the left so that the value of 2θ becomes smaller. According to the Bragg equation, the interplanar spacing is the reason for the decrease in 2θ. The addition of Wfs changes the internal stress of the composites after sintering, thus affecting the interplanar plane spacing which results in the shift of the diffraction peak. So, the crystal lattice of Al is deformed due to the influence of Wfs.

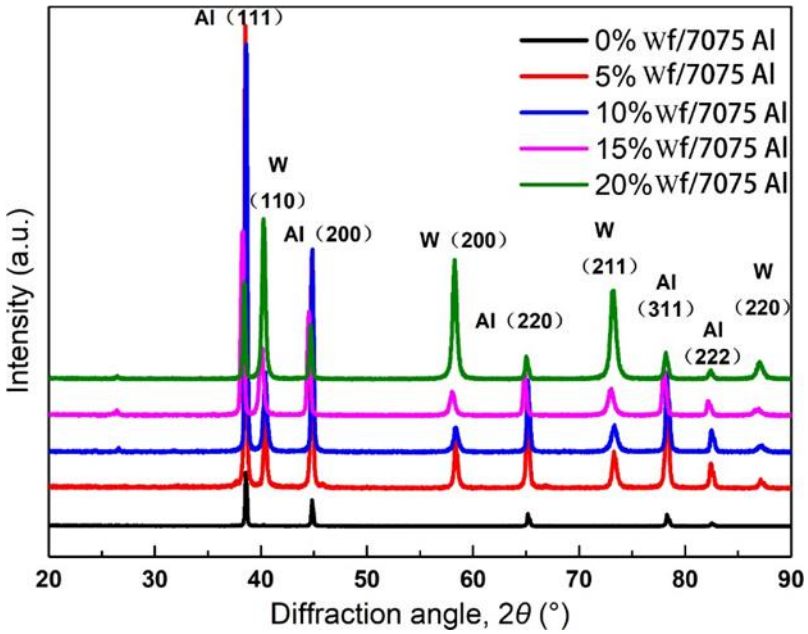

Figure 1. The XRD patterns of the Wf/7075Al composites produced under different Wfs mass percent.

3.2 Microstructural characterization

For discontinuously reinforced composites material, the most important factor is the uniform dispersion of the reinforcement, ensure homogeneous properties are implemented. Therefore, the homogeneity of the reinforcing phase in the composite could be determined by the appearance of the microstructure [16]. Fig. 2 and Fig. 3 demonstrate the OM micrograph of the experimental composites. The white area characterized Wfs, whereas the black area exposed the matrix of 7075 Al. In Fig. 2, the microstructure observations revealed that there were defect or porous cluster at some locations in the matrix, and the Wfs were different in shape horizontally, longitudinally or at an angle. The distribution of Wfs was reasonably more uniform throughout the Wf/7075Al composites with the increase of Wfs content. Because it is difficult to mix particles and fibers evenly, the distribution of Wfs was inhomogeneous when the fiber content is low. The porosity may be attributed to the air bubbles sucked into the mixture during mechanical mix Wfs in the 7075 Al powder. But the porosity of the 5%Wf/7075Al in Fig. 2B was less than Fig. 2A. Tab. 2 shown the density of Wf/7075Al composites which consistent with the results of Fig. 2. As shown in Tab.1, the relative density of Wf/7075Al composites with Wfs content of 5%, 10%, 15% and 20% is 98.83%, 96.68%, 91.82%, 89.21%. The relative density K was calculated according to the Archimedes principle. The calculation formula is as follows:

$$K = \rho r \rho f \rho a \quad \rho\ am f + ma \rho f \tag{1}$$

where ρr is the actual density, ρf the density of tungsten fibre, ρa is theoretical density of 7075 Al alloy, ma is the mass of matrix, mf is the mass of tungsten fibre.

Maybe the Wfs influences the spark plasma generated, improve the density of the matrix. So the 5%Wf/7075Al was more dense than pure 7075 Al alloy. Wfs should be resisted the greater pressure while the content of Wfs was higher, Meanwhile, the smaller the pressure borne of the matrix, which resulted in the higher the porosity of the matrix. So the degree of porosity was found more in the Wf/7075Al composites, and the porosity increased as the reinforcement content increases.

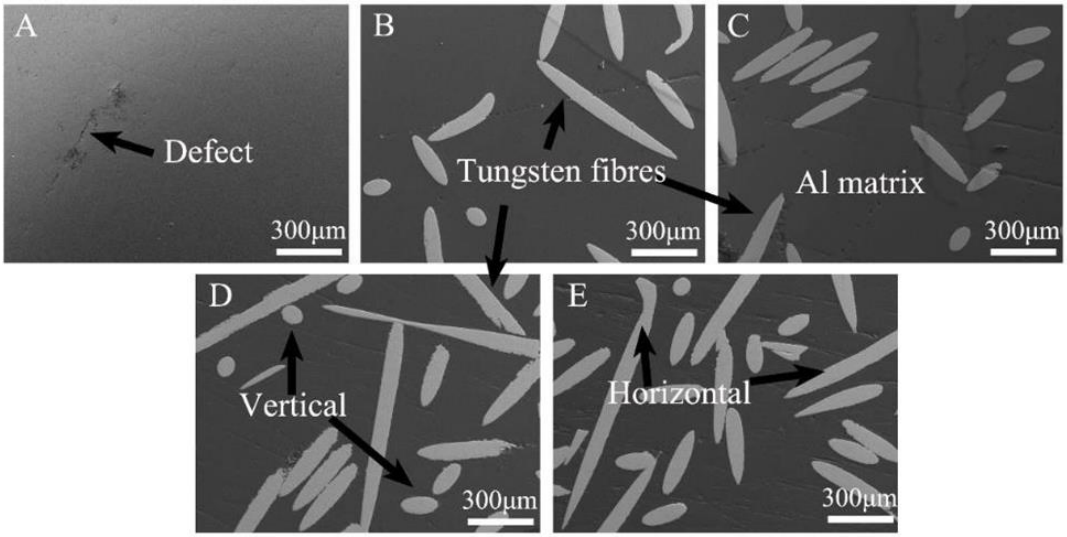

Figure 2. Optical micrograph of Wf/7075Al composites A: 7070Al; B: 5%Wf/7075Al composites; C: 10%Wf/7075Al composites; D: 15%Wf/7075Al composites; E: 20%Wf/7075Al composites.

Table 2. Relative density of Wf/7075Al composites

W/Wf%	0%	5%	10%	15%	20%
Relative density	96.21%	98.83%	96.68%	91.82%	89.21%

In order to analyze the interface of Wf/7075Al composites, the optical micrograph with greater enlargement of 10%Wf/7075Al composites was shown in Fig. 3. As shown in the picture, the shapes of Wfs are different. The interface between whether transverse (Fig. 3A) or longitudinal (Fig. 3B) Wfs and Al alloy was relatively tight. When the spacing of Wfs is similar, the matrix particles can enter the gap between Wfs to form a dense interface (Fig. 3C). The interface at fibre/matrix can be observed more clearly in Fig. 3D, 3E, and 3F. The ellipse area in Fig. 3D and Fig. 3F shows that the second phase or impurities gather at the interface between Wfs and matrix, which is difficult to avoid in the powder metallurgy process [17]. Maybe the Wfs affected the aggregation of impurities. Meanwhile, perfect interface with no impurities was observed in rectangle area of the Figs. 3E and 3F.

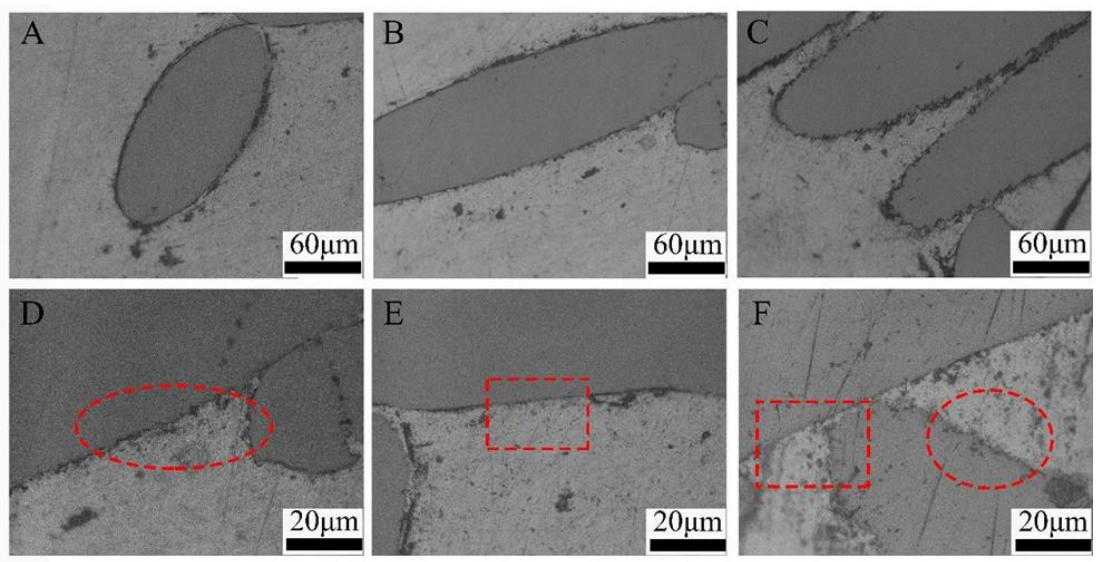

Figure 3. The interface of optical micrograph in 10%Wf/7075Al composites. The ellipse area and rectangle area: interface.

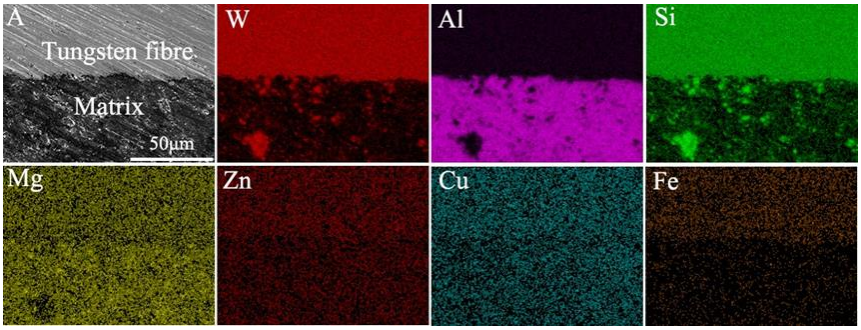

Figure 4. The EDS spectra of 10%Wf/7075Al composites. A: Scan area and the others are the element distribution map, and the element types are marked in the upper left corner.

As we all know, the wettability is poor between tungsten and Al [18], so it is difficult to achieve a close interface between Wfs and Al alloy matrix. However, Fig. 3 has proved that there is a close interface between the Wfs and the 7075 Al alloy matrix by SPS. It is expected that some element in Al alloy could form intermetallic compounds with the Wfs. To verify this problem, the EDS spectra of 10%Wf/7075Al composites are shown in Fig. 4, which shows the element composition of the fibre in Fig. 4A. There is a higher content of Si, Mg, Zn, Cu, and Fe on the Wfs. It may maybe formed W-Si, Mg, Zn, Cu, and Fe alloy, thus the strength of the interface between the Wfs and Al alloy was improved. However, the W-Si alloy is not revealed in XRD pattern, probably the content of the phase is less or cannot be guaranteed in the test plane phase.

3.3 Mechanical property test

Tensile tests were performed at room temperature on Wfs reinforced 7075 Al composites with fibre content of 0, 5%, 10%, 15%, and 20%, and the curves of engineering stress versus strain were shown in Fig. 5. The pure 7075 Al alloy exhibited plastic deformation, the elongation was about 8% and the tensile strength was about 165MPa. However, the Wf/7075Al composites show high-strength tensile behavior and work-hardening. With the increase of Wfs content, the tensile strength of the composite increases. However, once the Wfs content exceeds 10%, the tensile strength decreases. The fracture strength of 10%Wf/7075Al composites can reach as high as 250 MPa, 72.4% higher than that of pure 7075 Al alloy. Among the four composite samples, the 10%Wf/7075Al sample exhibits the highest fracture strength and significant toughness. During the tensile tests, all phenomena such as fibre splitting (fibre crack), interface debonding, and frictional fibre pull-out are responsible for the high strength as characterized [15]. The mechanical properties of Wf/7075Al samples with up to 10% Wfs were improved while the composites with more tungsten fibre content like 15%Wf/7075Al and 20%Wf/7075Al composites show a decreasing strength and ductility, which may be due to the lower density. Due to the aluminum-based powder being unable enter the voids between tungsten wire, more gaps cannot be filled with the increase of tungsten wire content. When the tension is carried out, the gap becomes a crack source, which leads to the failure of the samples.

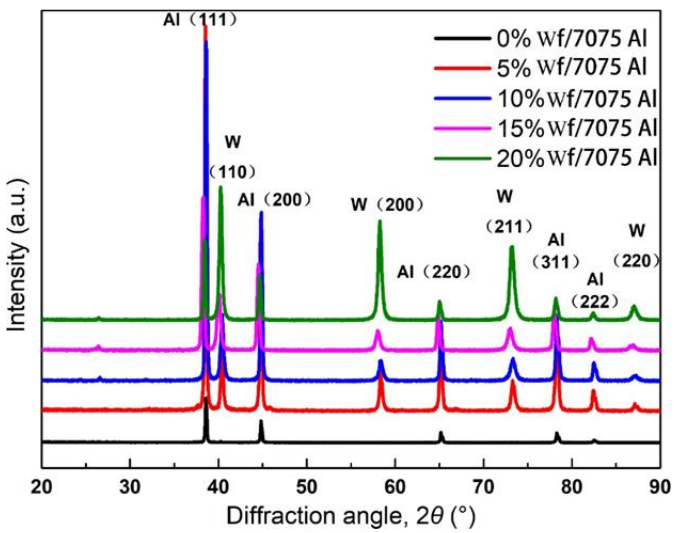

Figure 5. Engineering stress-strain curves of Wf/7075Al composites at room temperature.

The following expression can be used to predict the tensile strength σ of discontinuous fiber reinforced composite:

$$\sigma = \bar{\bar{\sigma f}}\varphi + (1 - \varphi) \quad (2)$$

where $\bar{\bar{\sigma f}}$ is the average strength of fiber, σm is the the strength of matrix, φ is the volume fraction of tungsten fibre. However, there is a difference of tungsten fiber and Al matrix strength large. The maximum tensile stress cannot reach the average strength of fiber, and the fiber will not break. The failure is caused by the damage of interface or matrix. Therefore, the calculation formula of composite tensile strength is converted as follows:

$$\sigma = \bar{\bar{\sigma b}}\varphi b + (1 - \varphi b) \quad (3)$$

where

$\bar{\bar{\sigma b}}$ is the average strength of the interface, φb is the volume fraction of the interface.

The hardness of the matrix, fibre, and interface in composites is shown in Fig. 6. Each group of data is the average value of the test, and the maximum error is about 5 HV. It is interesting to note that the hardness of the matrix was only between 50 and 60 HV, even smaller than that of fibre (about 1100 HV) and interface (1400 HV). The hardness of the interface is highest. It can be seen that the hardness of the matrix, fibre, and interface is slightly increased from pure 7075 Al alloy to 5%Wf/7075Al composites, and then decreased, due to the density of the samples, which is in agreement with the OM and the tensile test.

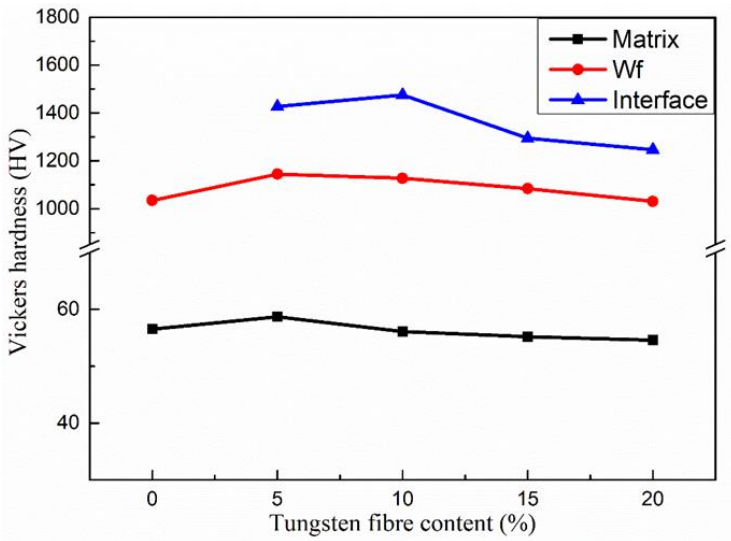

Figure 6. Vickers hardness curves of Wf/7075Al composites with matrix, fibre, and interface.

4. Conclusions

Tungsten fibre reinforced 7075 Al composites (Wf/7075Al) with enhanced hardness and denstiy are produced by SPS method. Four kinds of composites with different content Wfs of 5%, 10%, 15%, and 20% are investigated in comparison with pure 7075 Al alloy. The interface of all the composites has good bonding between the fibre and matrix. The Si, Mg, Zn, Cu, and Fe of the matrix were radiated out to the Wfs. The density decreases with the increase of Wfs content. The results indicate that tungsten fibre reinforcement can effectively strengthen the 7075 Al matrix.

Funding

This work was financed by the Natural Science Foundation of Qinghai Province under Grant No. 2020-ZJ-933Q and the Aluminum Corporation of China Limited Qinghai Branch.

Author Contributions

L.Z. took out the original ideas, carried out all the experiments, and prepared the draft of the manuscript. B.Z. modified the manuscript and gave suggestions in the discussion. Y.X carried out the experiments.

References

[1] Wu Y C, Zhao Y K, Ma C H, et al. International radioactive waste disposal policy and experience enlightenment [J]. Journal of the Chinese Academy of Sciences, 2020, 35(01): 99-111.

[2] Zou S, Kuang Y, Tang D, et al. Risk analysis of high level radioactive waste storage tank based on HAZOP [J]. Annals of Nuclear Energy, 2018, 119: 106-116.

[3] Wang J. High-level radioactive waste disposal in China: update 2010 [J]. Journal of Rock Mechanics and Geotechnical Engineering, 2010, 2: 1-11.

[4] Li J, Chen L, Wang J. Solidification of radioactive wastes by cement-based materials [J]. Progress in Nuclear Energy, 2021, 141: 103957.

[5] Xiong Y, Wang Y, Roselle G, et al. Lead/lead-alloy as a corrosion-resistant outer layer packaging material for high level nuclear waste disposal [J]. Nuclear Engineering and Design, 2021, 380: 111294.

[6] Guo X, Gin S, Lei P, et al. Self-accelerated corrosion of nuclear waste forms at material interfaces [J]. Nature Materials, 2020, 19: 310-316.

[7] Zhang B. High resolution γ Application of energy spectrum logging in pollution assessment [J]. Foreign Uranium and Gold Geology, 1997, 14 (4): 367-378.

[8] Chen X W, Li M L, Zhang D F, et al. Corrosion resistance of MoS2-modified titanium alloy micro-arc oxidation coating [J]. Surface and Coatings Technology, 2022, 433: 128127.

[9] Dunn D S, Cragnolino G A, Sridhar N. An electrochemical approach to predicting long-term localized corrosion of corrosion-resistant high-level waste container materials [J]. Corrosion, 2000, 56: 90-104.

[10] Frankel G S, Vienna J D, Lian J, et al. Recent Advances in Corrosion Science Applicable to Disposal of High-Level Nuclear Waste [J]. Chemical Reviews, 2021:1-57.

[11] Mohri M, Odagiri H, Satake T, et al. Surface characterization of aluminum alloy 2017 as a vacuum vessel for nuclear fusion devices [J]. Journal of Nuclear Materials, 1984, 122(1-3): 164-168.

[12] Zhang X, Xiao Z, Zhu L, et al. Influence of erbium addition on the defects of selective laser-melted 7075 Aluminium alloy [J]. Virtual and Physical Prototyping, 2022, 17(2): 406-418.

[13] Saeidabadi E K, Gholamipour R, Ghasemi B. Effect of melt infiltration parameters on microstructure and mechanical properties of tungsten wire reinforced (Cu50Zr43Al7)99.5Si0.5 metallic glass matrix composite [J]. Transactions of Nonferrous Metals Society of China, 2015, 25(8): 2624-2629.

[14] Tokita M. Progress of Spark Plasma Sintering (SPS) Method, Systems, Ceramics Applications and Industrialization [J]. Ceramics, 2021, 4:160-198.

[15] L. H, Zhang, Y, et al. Toughness and microstructure of tungsten wire net-reinforced tungsten composite produced by spark plasma sintering [J]. Materials Science and Engineering: A, 2016, 659: 29-36.

[16] Yigezu B S, Mahapatra M M, Jha P K. Influence of Reinforcement Type on Microstructure, Hardness, and Tensile Properties of an Aluminum Alloy Metal Matrix Composite [J]. Journal of Minerals & Materials Characterization & Engineering, 2013, 01(4):124-130.

[17] Queeney R. Advances in Powder Metallurgy and Particulate Materials [J]. Industrial Lubrication and Tribology, 1998, 50(3): 71-83.

[18] Lafeng Guo, Zhimin Zhang, Baocheng Li, et al. Modeling the constitutive relationship of powder metallurgy Al–W alloy at elevated temperature [J]. Materials & Design, 2014, 64: 667-674.